frontiers in Materials

ORIGINAL RESEARCH
published: 15 April 2019
doi: 10.3389/fmats.2019.00052

# *In-situ* Construction of Superhydrophilic g-$C_3N_4$ Film by Vapor-Assisted Confined Deposition for Photocatalysis

*Fuhao Jia, Yizhu Zhang, Wenjuan Hu, Min Lv, Changchao Jia and Jian Liu**

*College of Materials Science and Engineering, Qingdao University of Science and Technology, Qingdao, China*

Herein, we report an improved strategy for the synthesis of superhydrophilic g-$C_3N_4$ film by vapor-assisted confined deposition method. With minimum amount of precursor, the vapor could be confined in the microenvironment for facilitating the film growth on both sides of the substrates. The obtained films showed similar physiochemical properties with the bulk counterpart and could be peeled off from the substrates by soaking in hot water. The free-standing film is flexible and superhydrophilic, featuring many microfibers atop. The g-$C_3N_4$ film from both sides of the substrates could be used in the photocatalytic dye degradation in a repeated manner and showed excellent performance and stability. The current work should shed light on the optimized growth of the g-$C_3N_4$ film and could find more application in future device field.

**Keywords: g-$C_3N_4$ film, photocatalysis, vapor-assisted, confined deposition, superhydrophilic**

OPEN ACCESS

***Edited by:***
*Xin-Hao Li,*
*Shanghai Jiao Tong University, China*

***Reviewed by:***
*Xiaofeng Liu,*
*Zhejiang University, China*
*Jingsan Xu,*
*Queensland University of Technology, Australia*

****Correspondence:***
*Jian Liu*
*liujian@qust.edu.cn*

***Specialty section:***
*This article was submitted to Colloidal Materials and Interfaces, a section of the journal Frontiers in Materials*

***Received:*** *20 February 2019*
***Accepted:*** *14 March 2019*
***Published:*** *15 April 2019*

***Citation:***
*Jia F, Zhang Y, Hu W, Lv M, Jia C and Liu J (2019) In-situ Construction of Superhydrophilic g-$C_3N_4$ Film by Vapor-Assisted Confined Deposition for Photocatalysis. Front. Mater. 6:52. doi: 10.3389/fmats.2019.00052*

## INTRODUCTION

g-$C_3N_4$ is a promising metal-free conjugated polymer featuring several advantages, including earth-abundant composition, high stability, high visible light absorption efficiency, and favorable band energy levels (Wang et al., 2009). All these properties make g-$C_3N_4$ a promising candidate for catalytic and conventional applications in the last decade (Thomas et al., 2008; Wang et al., 2012; Liu et al., 2016b; Ong et al., 2016). Numerous studies were put into improving the catalytic efficiencies of g-$C_3N_4$ through strategies including nanoarchitectures design, functionalization through molecular engineering and modification with other semiconductors or metals (Sun et al., 2012; Jun et al., 2013; Liu and Antonietti, 2013; Huang et al., 2014, 2018; Liu et al., 2014a,b, 2015a, 2016c, 2017a,b, 2018; Shalom et al., 2014; Cao et al., 2015a; Han et al., 2015; Yang et al., 2015b; Xiong et al., 2016; Zhou et al., 2016; Ong, 2017; Xia et al., 2017; Xu et al., 2017; Yu et al., 2017; Chen et al., 2018a,b, 2019; Choi et al., 2018; He et al., 2018; Zhao et al., 2018; Zhang et al., 2019). The heterogeneous nature of the g-$C_3N_4$ powder necessitates the development of the film for further practical device use (Cazelles et al., 2015; Chen et al., 2018b; Xiao et al., 2019; Xu and Shalom, 2019). Inspired by the tremendous progresses in the conjugated polymer field, g-$C_3N_4$ can be utilized as the organic layer in optoelectronic devices (solar cells, light-emitting diodes) and photoelectrochemical cells (Xu et al., 2014, 2015b,c; Jiang et al., 2018). Nevertheless, the growth of uniform, high-quality g-$C_3N_4$ thin films has proven very challenging, which severely limits the practical application of g-$C_3N_4$ based devices.

Initially, people adopted the conventional two-step methods such as spin-coating or electrophoretic to make the g-$C_3N_4$ film photoelectrode (Chen et al., 2009; Zhang et al., 2010, 2012, 2015; Martha et al., 2013). However, g-$C_3N_4$ materials does not usually dissolve in common solvents or can't form stable colloid solution with ultrafine particles, rendering conventional methods not totally suitable for g-$C_3N_4$ thin film fabrication. After the initial efforts through two-step routes, more and more works are aiming at obtaining the film directly from *in-situ* thermal condensation. Some specific approaches have been developed to deposit g-$C_3N_4$ films. Recently, several groups pioneered the design and synthesis of the g-$C_3N_4$ film by *in-situ* method, which could avoid the poor interfacial engineering problem usually occurred in the conventional two-step deposition methods. For example, Xu et al. reported a liquid-mediated method for the synthesis of electrode (Xu et al., 2014). Liu et al. reported a AAO templated growth of hierarchical film with nanostructures on glass or FTO substrates (Liu et al., 2015b). Bian et al. deposited a thin layer onto the conductive substrates by placing the substrates onto the mouth of the crucible (Bian et al., 2015a). Aida et al. reported a vapor-assisted polymerization method for the deposition of the film for actuator applications (Arazoe et al., 2016). Tang et al. reported a one-step synthesis of metal-free photoanode nanojunction architecture, composed of B-doped carbon nitride nanolayer, and bulk carbon nitride (Ruan et al., 2017). Actually, all the film formation are based on the vapor deposition during heating of precursors, partially sublimed and then deposited onto the substrate surface (Arazoe et al., 2016; Xiao et al., 2018). Wang and Dai et al. reported a $CCl_4$ assisted method to construct free-standing g-$C_3N_4$ films by using *in-situ* extracted metal cations as nucleate sites (Li et al., in press). By placing the substrates in the vicinity of the precursor source, the film could be obtained on the substrate by *in-situ* deposition. However, in the previous reports, several grams of melamine (or other precursors) usually has to be adopted for the film formation (Bian et al., 2015a,b; Xu et al., 2015a; Arazoe et al., 2016; Ye and Chen, 2016; Lu et al., 2017; Lv et al., 2017; Peng et al., 2018; Xiao et al., 2018, 2019; Xiong et al., 2018). Most of the precursor can't be converted to the film, although there are indeed plenty of bulky carbon nitride formed in the bottom of the crucible. Reducing the needed amount of the precursor and also improving the film formation could make the application of film-based device more feasible and practical.

Herein, we reported an improved route to synthesize the g-$C_3N_4$ film through a confined strategy (Bian et al., 2015b; Liu et al., 2015b; Xiao et al., 2019). Specifically, the substrates were covered onto the crucible containing minimum amount of melamine and urea (Martha et al., 2013; Liao et al., 2014). The whole setup was then wrapped by a layer of aluminum foil to form a confined environment. After thermal condensation, the film could be obtained in the substrates and peeled off from both sides of the substrates by soaking in the hot water. Interestingly, the microfibers with several micrometers long could be observed on top of the film. The g-$C_3N_4$ film demonstrates similar physiochemical properties with the bulk counterpart. The performances of the films from different sides were compared and showed no apparent difference. The morphologies were slightly different for the upward and downward sides. The freestanding and superhydrophilic films were used in the photocatalytic degradation of Rhodamine B (RhB). Due to the mechanical strength of the film, it could be directly reused for at least four consecutive times without any damage and performance degradation. The work reported herein could provide a practical solution for the device application of the g-$C_3N_4$ film based materials.

# EXPERIMENTAL

## Synthesis of g-$C_3N_4$ Films on Glass

The synthesis of g-$C_3N_4$ films on glass substrate is described as follows. Firstly, 3 equivalent of melamine and 1 equivalent of urea were mixed together and ground well in a mortar. Second, 50 mg of the mixture was placed into a ceramic crucible with the cleaned glass substrate covering the top. Then the entire setup was wrapped by aluminum foil. Then, the wrapped ceramic crucible was transferred into tube furnace and kept in 550°C for 4 h under $N_2$ atmosphere with a heating ramp of 2.3°C/min. After cooling down to room temperature, g-$C_3N_4$ films were deposited on the both of upward side and down side of glass, while yellow g-$C_3N_4$ powder was obtained from the bottom of ceramic crucible. Similarly, the thickness of g-$C_3N_4$ films can be changed by adjusting the amounts of precursor placed in the crucible.

## Characterization

The morphology of as-prepared g-$C_3N_4$ films were characterized by JSM-7500F field-emission scanning electron microscopy. The crystalline of as-prepared g-$C_3N_4$ films were measured by X-ray diffraction using Cu Kα source radiation. Two theta Diffraction angles ranged from 10 to 60 degree, and the scanning step was 0.02 degree. X-ray photoelectron spectroscopy (XPS) data was obtained from Thermo ESCALAB 250 using 150 W Al Kα radiation. The binding energies were referenced to the C1s line at 284.8 eV from adventitious carbon. The UV-vis absorption spectra of samples were obtained from a Hitachi U-3900 spectrophotometer equipped with an integrating sphere. The photoluminescence (PL) spectra were excited at room temperature using He-Cd laser (365 nm) (Thermo Scientific). Contact angle measurements were performed on Lauda LSA 60 Surface Analyzer.

## Photocatalytic Experiments

The photocatalytic activity of the sample was evaluated by degradation of RhB under white light LED with irradiation intensity of 175 mW/cm$^2$. Typically, 15 mL of aqueous RhB solution (5 mg·L$^{-1}$) was added into a beaker containing g-$C_3N_4$ film (3.5 cm × 5 cm, about 1.3 mg) and refluxed with condensed water. Before light irradiation, the film was kept in the dark for 1 h to reach adsorption-desorption equilibrium. The changes of RhB concentration were monitored through UV-vis absorption spectra at 552 nm which corresponds to the characteristic absorption peak of RhB. After completing a cycle, the g-$C_3N_4$ film was rinsed three times with deionized water carefully. Deionized water was removed from container

with a pipette following with extensive rinse. The cleaned and dried g-$C_3N_4$ film could be applied for the repeated degradation experiments.

## RESULTS AND DISCUSSION

Herein, we reported the synthesis of microstructured g-$C_3N_4$ film by a confined strategy. The typical process for deposition of g-$C_3N_4$ film on glass substrate is schematically shown in **Scheme 1**. The aluminum foil wrapping from the outside of the crucible could form a confined space for facilitating the vapor deposition with minimum amount of precursor. Different ratios of melamine and urea were employed to deposit the g-$C_3N_4$ films. It is found that the uniform g-$C_3N_4$ film could be obtained when the ratio of melamine to urea was 3:1 (see **Figure S1**). As illustrated in **Table S1**, most of the previous reports used at least half gram of melamine or other nitrogen-rich precursor for deposition (Bian et al., 2015a,b; Xu et al., 2015a; Arazoe et al., 2016; Ye and Chen, 2016; Lu et al., 2017; Lv et al., 2017; Peng et al., 2018; Xiao et al., 2018, 2019; Xiong et al., 2018). Most of the precursor can't be converted to the film. In our case, 50 mg of precursor mixture was employed and placed in the bottom of crucible. The condensation process is as follows: urea is condensed to melamine at low temperature; when the heating temperature exceeds 300°C, the vapor of both melamine and urea were obtained; further heating to 390 °C, the tri-*s*-triazine units formed through rearrangements of melamine. Eventually, carbon nitride films could be obtained on the glass substrate (Wang et al., 2009). It is worth mentioning that melamine alone cannot form uniform carbon nitride film (**Figure S1a**), suggesting that urea might play an essential role in thermal condensation.

By soaking in hot water, g-$C_3N_4$ film can be stripped off from glass substrates (Liu et al., 2015b; Arazoe et al., 2016). Two pieces of freestanding g-$C_3N_4$ film are obtained from both sides of the glass substrate. To the best of our knowledge, the double-sides film deposition of g-$C_3N_4$ on the substrates is rarely reported. Presumably, the space between the aluminum foil and the glass provides a microenvironment for the deposition of g-$C_3N_4$ films. It's speculated that the vapor could spread from the gap between the glass and the ceramic crucible to the upward side of glass for further deposition (Bian et al., 2015b). For simplicity, the g-$C_3N_4$ films which are obtained from the upward and downward side of glass substrate are abbreviated as CNFD and CNFU, respectively.

The SEM images in **Figures 1a,b** display the morphologies of free-standing g-$C_3N_4$ films showing a certain bending property. From **Figures 1a–d**, it's clear that the side in contact with the glass is a featureless conformal coating, while dense of microfibers or microbump are distributed on the opposite side (see also **Figure S2**). There are also large differences between CNFU and CNFD, respectively. For CNFD, denser of microfibers with diameters in the range of 150–200 nm and length in the range of 3–4 μm could be obtained (**Figures 1c,e**). The length to diameter ratio is estimated in the range of 15–25, which contributes to high surface roughness. This rough morphology might enhance the light harvesting that could be beneficial for photocatalysis (Liu et al., 2009, 2010; Yang et al., 2015a). For CNFU, irregular and random microbump particles and microfibers were observed (**Figure 1d** and **Figure S2b**). The morphology differences between CNFU and CNFD are ascribed to the slightly different deposition environment. The corresponding cross-section image demonstrates a continuous ultrathin g-$C_3N_4$ film with thickness of about 150 nm (**Figure 1e**). For comparison, the thickness of CNFU can reach to roughly 350 nm (**Figure 1f**). It is feasible that the delaminated film can be transferred to other flexible substrate which cannot sustain high temperatures, extending its potential application on flexible electronics.

Most of the previous works reported on the film formation was exclusively on the flat thin film without apparent micro-/nanoarchitectures (Arazoe et al., 2016; Xiao et al., 2018). However, the direct growth of microfibers and nanowires were frequently reported before. The leading author of the current work previously reported a diatom templated growth of g-$C_3N_4$ nanowires, nanocluster, and nanoribbons (Liu et al., 2013a). Zhao et al. reported the synthesis of carbon nitride microfibers using g-$C_3N_4$ as the precursor and ascribed the direct growth of the microstructures to the vapor-solid mechanism (Zhao et al., 2008). As well-known, for one-dimensional material, the growth mechanism satisfies vapor-liquid-solid mechanism in the presence of catalysts while vapor-solid (VS) mechanism prevails without catalysts (Zhao et al., 2008; Liu et al., 2013a). In the current case, the latter VS growth mechanism should be applied for the growth of microfibers on top of the film. The supersaturation of the precursor in the vapor-solid mechanism determines the morphology of the film. One-dimensional structure was obtained at low supersaturation, while bulk material was obtained at high supersaturation. To further reveal the growth mechanism of microfibers, control experiments were performed by adding more precursors. One hundred milligram instead of 50 mg of precursor was placed into the ceramic crucible for film deposition. After thermal condensation, the morphology of the obtained g-$C_3N_4$ film shows irregular spherical-like microparticles (**Figure S3a**). However, there are still a bunch of microfibers deposited on film (**Figure S3b**). Besides, some micrometer-scale bumps highlighted in red boxes can be distinguished on the spherical particles, suggesting that the micrometer-scale bumps may evolve into microfibers (Zhao et al., 2008). The same micrometer-scale bumps can also be observed on the surface of CNFD (**Figure 1e**). This indicates that micrometer-scale bumps may play an important role in inducing the formation and growth of microfibers.

Based on the above results, it's speculated that the growth mechanism of microfibers is as follows: the evaporated vapor from melamine and urea precursor is carried upward by the $N_2$ gas flow and then the vapor diffuses to the glass surface to nucleate. The vapor nucleates easily and uniformly on the surface of the glass, which is vital for deposition of uniform g-$C_3N_4$ films. As a result of the temperature difference between the film surface and the vapor, the deposition starts to occur, which is beneficial to form micrometer-scale bumps and rough surface. After formation of micrometer-scale bumps, g-$C_3N_4$ will grow along with direction of the bump directly leading to the formation of microfibers. The schematic illustration of the

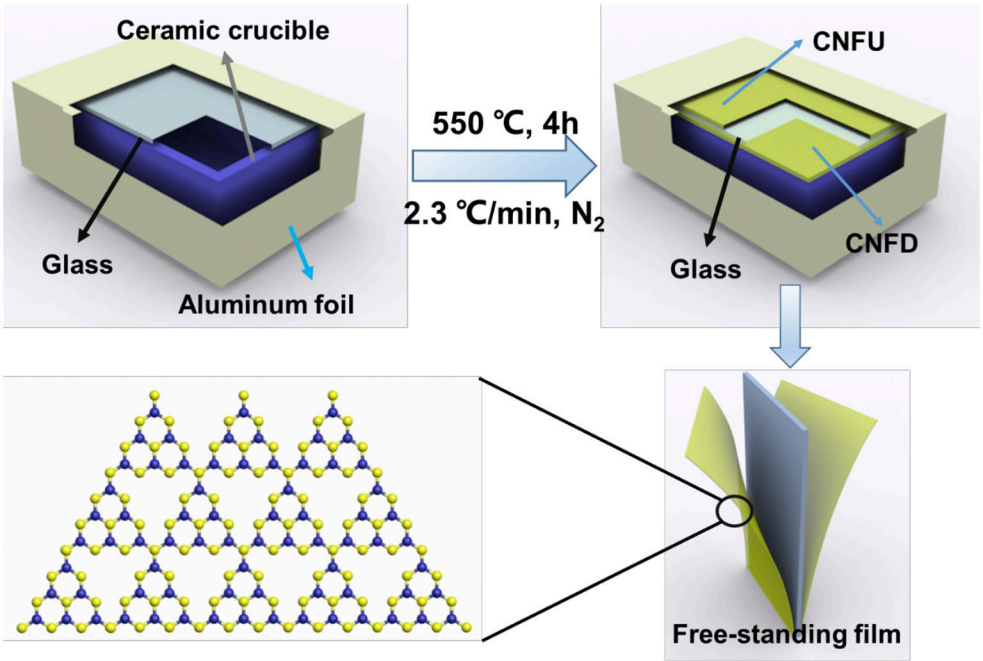


**SCHEME 1 |** Schematic illustration for synthesis of g-$C_3N_4$ film by vapor-assisted confined deposition.

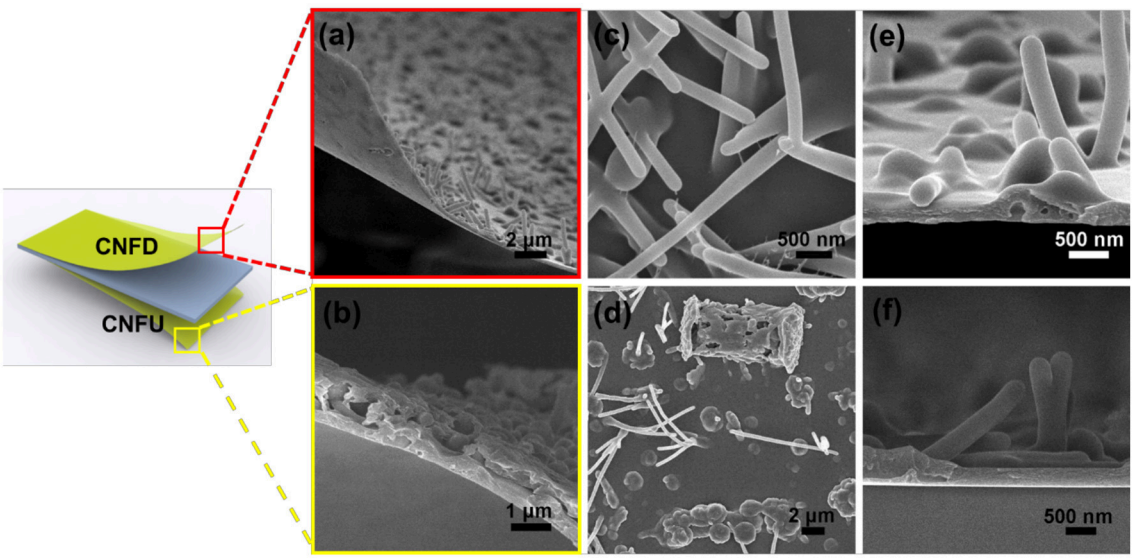


**FIGURE 1 |** SEM images of g-$C_3N_4$ films. Overall views of CNFD **(a)** and CNFU **(b)**, top views of CNFD **(c)** and CNFU **(d)**, and cross section view of CNFD **(e)** and CNFU **(f)**, respectively.

deposition process is shown in **Scheme S1**. In brief, the successful synthesis of microfibers could be attributed to the formation of uniform nucleation and micrometer-scale bumps.

The crystallinity of the delaminated g-$C_3N_4$ film and powder were analyzed by XRD and the corresponding results are shown in **Figure 2A**. The diffraction peaks of bulk powder with strong intensity located at 27.5 ° and 13.1 ° could be ascribed to the typical graphitic interlayer (002) plane and the in-plane structural repeating unit of the aromatic systems, respectively. The free-standing film shows a broad peak at 27 ° while the peak of (100) plan disappeared. Fourier transform infrared spectroscopy (FTIR) measurement of the g-$C_3N_4$ film on glass is shown in

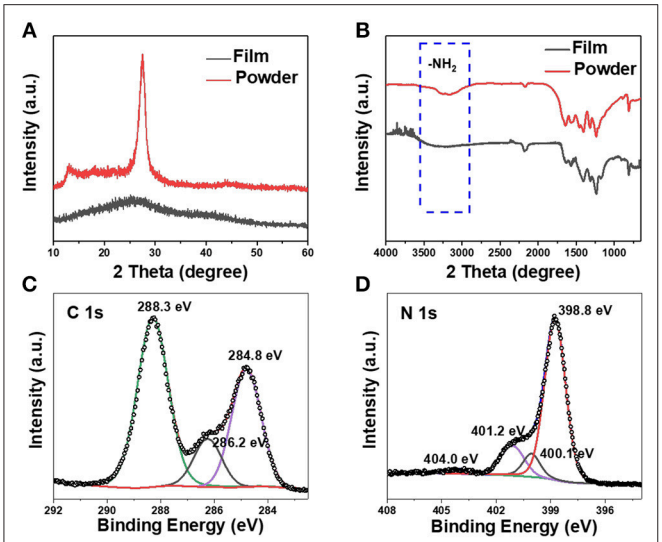


**FIGURE 2 | (A)** XRD patterns and **(B)** FTIR spectra of g-$C_3N_4$ film and powder. Typical C1s **(C)** and N1s **(D)** XPS spectra of g-$C_3N_4$ film.

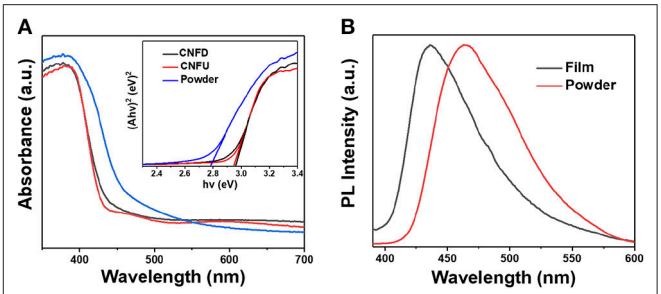


**FIGURE 3 | (A)** UV-vis absorption spectra of g-$C_3N_4$ films and powder (inset showing the corresponding Tauc plots), **(B)** Normalized photoluminescence spectra of the film and bulk powder.

**Figure 2B**. The FTIR spectra of both film and powder samples show the typical breathing mode at about 810 $cm^{-1}$, which is the characteristic absorption peak of the triazine unit in carbon nitride. The characteristic stretching modes of the C-N heterocycles was observed ranging from 1170 to 1630 $cm^{-1}$. The peak at 2,180 $cm^{-1}$ correspond to an asymmetric stretching vibration of cyano groups (-C=N). The absorption peaks between 2900 and 3600 $cm^{-1}$ are -$NH_2$ groups. It is worth mentioning that no obvious differences can be found between the g-$C_3N_4$ film and powder in the FTIR spectra, confirming the formation of g-$C_3N_4$ structure. The above results matched well with previously reported values for g-$C_3N_4$ with heptazine as a building bock. The oxidation states and surface elemental composition of the g-$C_3N_4$ film were investigated by X-ray photoelectron spectroscopy (XPS). The survey of XPS spectrum mainly detected three elements (C, N, O) in the film (**Figure S4a**). The oxygen is ascribed to the absorbed water on the surface of the carbon nitride film (**Figure S4b**).

As displayed in **Figure 2C**, three fitting peaks located at 284.8, 286.2, and 288.3 eV were observed, which are corresponding to the graphitic carbon (C-C), the $sp^2$-type C=N bonds and $sp^2$ hybridized carbon in tri-*s*-triazine rings ($N_2$-C=N), respectively. The N 1s spectrum in **Figure 2D** can be deconvoluted into four peaks corresponding to nitrogen atoms in different functional groups: $sp^2$ hybridized aromatic N bonded to carbon atoms of the *s*-triazine ring at 398.8 eV, tertiary N bonded to carbon atoms in the form of N-$(C)_3$ at 400.3 eV, amino functional groups with hydrogen (C-N-H) at 401.2 eV, and pi-excitations at 404.0 eV (Cao et al., 2015b). The XPS spectra demonstrate the presence of the tri-*s*-triazine units, which is agreement with FTIR spectra.

The UV-vis diffuse reflectance absorbance spectra of the g-$C_3N_4$ films and bulk powder were shown in **Figure 3A**. The bulk powder shows an absorption edge at 469 nm, while the absorption edge of CNFD and CNFU sample blue shifted to 440 nm. For CNFD and CNFU, the absorption edge has no obvious difference, indicating identical optical properties. The band gap was calculated to be 2.78 eV and 2.95 eV for powder and film, respectively (see inset of **Figure 3A**). The blue-shift of the g-$C_3N_4$ film may be ascribed to the decreased condensation degree of the precursor. The calculated band gap of g-$C_3N_4$ powder prepared by melamine and urea is larger than g-$C_3N_4$ powder (2.73 eV) prepared by melamine, but smaller than the g-$C_3N_4$ powder (2.87 eV) prepared by urea (**Figure S5a**), suggesting that the band gap and electronic structure of the sample can be adjusted by co-condensation with urea.

The optical properties of the as-prepared g-$C_3N_4$ film and bulk powder were further studied by photoluminescence (PL) at an excitation wavelength of 365 nm (**Figure 3B**). The bulk powder of g-$C_3N_4$ showed a strong PL emission centered at about 463 nm while the emission peak of g-$C_3N_4$ film centered at about 435 nm, which is corresponding to the absorption edges in UV-vis diffuse reflectance spectra. Although both of CNFD and CNFU had the same emission peak (**Figure S5b**), the emission intensity of CNFU is stronger than CNFD, indicating the low charge separation efficiency of photogenerated electron-hole pairs of CNFU.

Few works have investigated the wettability of g-$C_3N_4$ before (Lin et al., 2019). The hydrophilic behaviors of the g-$C_3N_4$ films are very important for the photocatalysis since surface wettability influences the effective contact between the photocatalyst and the reactant solution (Sheng et al., 2017; Wu et al., 2018). The wettability was investigated by contact angel measurements, as illustrated in **Figure 4**. The as-prepared g-$C_3N_4$ films are proven to be superhydrophilic. When a water droplet (2 μL) was deposited on CNFD, it quickly infiltrated the surface, reaching a contact angle of 36.7° in < 0.05 s and 14.1° after 0.40 s. Finally, the droplet spread out completely and the contact angle decreased to 0° (i.e., superhydrophilic) within 2 s (**Figure 4A**). Similarly, CNFU exhibits similar superhydrophilic properties (**Figure 4B**). The contact angle decreased to 5.7° at 0.8 s and the water droplet spread out completely within 3 s. Water droplet spread faster on CNFD than on CDFU, presumably due to the difference of surface morphology. It is well-known that the

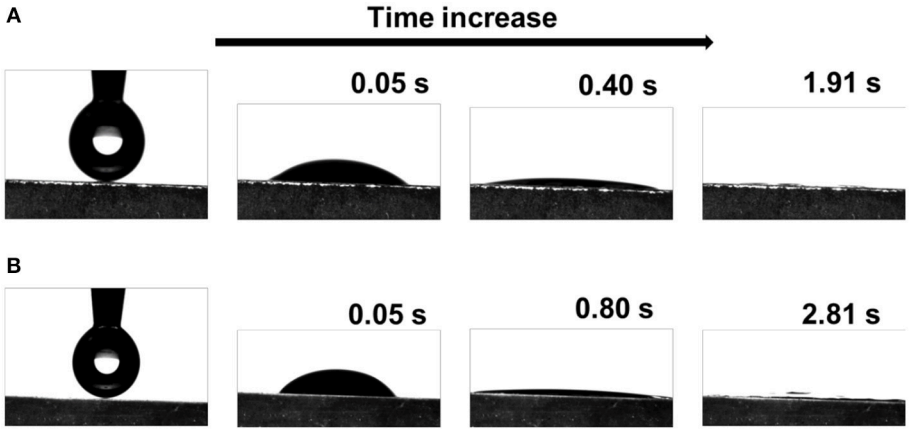


**FIGURE 4 |** Optical CA images of water on the g-$C_3N_4$ film, **(A)** CNFD, **(B)** CNFU.

topographic structure and the chemical composition of the surface govern the surface wettability. According to the Wenzel model (Wenzel, 1936), superhydrophilicity can be achieved by roughening a surface with intrinsic hydrophilic property. For the CNFD and CNFU sample, densely distributed microfibers and microbump particles contributed to enhanced roughness, respectively (see **Figure S2**). Besides, the layered structure of g-$C_3N_4$ is held together by van der Waals forces, and each layer consists of aromatic tri-*s*-triazine units. Due to incomplete condensation of the precursors, the residual amino groups that didn't participate in the condensation reaction could act as a hydrophilic group to ensures the intrinsic hydrophilicity of the g-$C_3N_4$ films. The existence of the residual amino group can be confirmed from FTIR spectra (**Figure 2B**). The synergy of surface roughness and the intrinsic hydrophilicity thus leads to superhydrophilicity of the as-prepared g-$C_3N_4$ films.

The degradation of RhB was tested under white light LED ($\lambda > 420$ nm, **Figure 5A**). The delaminated films possessed different photocatalytic activities. The control experiment indicates that the degradation of RhB under illumination didn't occur without photocatalysts (**Figure 5B**). For CNFD and CNFU, the degradation efficiency of RhB can reach to 96 and 87 %, respectively. The photocatalytic efficiency difference may partly be ascribed to the different surface morphologies between CNFD and CNFU. The lower PL intensity of CNFD suggested the higher charge separation efficiency, which could also contribute to the higher photocatalytic efficiency (**Figure S5b**). For comparison, an equal amount of powder with the film shows lower photocatalytic performance with degradation efficiency to 46% in the same period of time. Under stirring, the powder has a comparable photocatalytic activity with CNFU and the degradation efficiency could reach to 86%. After a cycle of degradation experiments, we measure the contact angle of CNFD and CNFU (as shown in **Figure S6**). Both of CNFD and CNFU exhibit excellent superhydrophilic property.

To investigate the recyclability of the g-$C_3N_4$ film, repeated degradation experiments were performed. The film photocatalyst

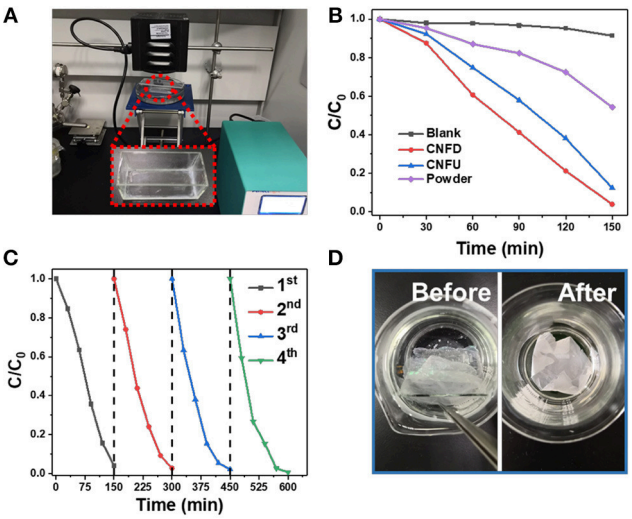


**FIGURE 5 | (A)** The employed photocatalytic degradation setup in the current work. **(B)** Photodegradation curves for RhB under white light LED. **(C)** Cyclic degradation experiments for CNFD under white light LED. **(D)** Digital photos of CNFD before **(left)** and after **(right)** four consecutive cycles.

could avoid the tedious collecting and cleaning steps usually occurred in the heterogeneous powder system (Yang et al., 2012; Liu et al., 2013b, 2016a, 2017b; Shan et al., 2019). After fourth cycle, CNFD and NFCF still maintain the similar catalytic performances (**Figure 5C**, **Figure S7b**). It is observed that the CNFD remained intact after fourth cycle (**Figure 5D**), demonstrating the excellent mechanical stability of this free-standing film. To further enhance the stability of the film, frosted glass was employed for g-$C_3N_4$ film deposition (abbreviated as NFCNF). The NFCNF film cannot be stripped off from the coarse substrate due to the enhanced roughness for strong binding the film with the substrate. NFCNF displays similar morphology (**Figure S7a**). As also shown in **Figure S8**, NFCNF maintained the nearly the same

morphology after the four cycles of RhB degradation test, also suggesting the high mechanical strength of NFCNF. For CNFD and NFCNF, the large aspect ratio of the microfibers provides a shorter path for electrons and holes to diffuse toward the surface. As a result, photogenerated electron-hole pair can be effectively separated. Compared with flat surface, the irregularly distributed microfibers contribute to high surface roughness with more reaction sites to react with dye molecules. Therefore, the enhanced photocatalytic activity of CNFD can be attributed to beneficial light harvesting and improvement in the charge-separation process.

## CONCLUSION

In summary, a confined strategy to deposit freestanding and ultrathin g-$C_3N_4$ film featuring with microfibers was demonstrated. The confined space provided by the wrapped aluminum foil ensured the minimum use of the precursor while also facilitating the growth of film on both sides of the substrates. The obtained g-$C_3N_4$ film display superhydrophilic property. By virtue of the mechanical strength and superhydrophilicity of the g-$C_3N_4$ film, it exhibits excellent photocatalytic activity and stability for the degradation of RhB in a repeated manner. The current work would shed light on the further investigation of the synthesis and application of the g-$C_3N_4$ film materials.

## DATA AVAILABILITY

The raw data supporting the conclusions of this manuscript will be made available by the authors, without undue reservation, to any qualified researcher.

## AUTHOR CONTRIBUTIONS

FJ and YZ contributed equally to the work. JL designed the experiment. FJ, YZ, WH, and ML synthesized and characterized the samples. FJ and CJ performed the photocatalytic experiments. JL, FJ, and CJ cowrote the manuscript. All authors have contributed to the discussion.

## ACKNOWLEDGMENTS

This work was financially supported by Natural Science Foundation of Shandong Province (ZR2018MB018). JL acknowledged Prof. Xuelin Tian of Sun Yat-sen University for kind suggestion.

## SUPPLEMENTARY MATERIAL

The Supplementary Material for this article can be found online at: https://www.frontiersin.org/articles/10.3389/fmats.2019.00052/full#supplementary-material

## REFERENCES

Arazoe, H., Miyajima, D., Akaike, K., Araoka, F., Sato, E., Hikima, T. et al. (2016). An autonomous actuator driven by fluctuations in ambient humidity. *Nat. Mater.* 15:1084. doi: 10.1038/NMAT4693

Bian, J., Li, J., Kalytchuk, S., Wang, Y., Li, Q., Lau, T. C. et al. (2015a). Efficient emission facilitated by multiple energy level transitions in uniform graphitic carbon nitride films deposited by thermal vapor condensation. *ChemPhysChem* 16, 954–959. doi: 10.1002/cphc.201402898

Bian, J., Qian, L., Chao, H., Li, J., Yao, G., Zaw, M. et al. (2015b). Thermal vapor condensation of uniform graphitic carbon nitride films with remarkable photocurrent density for photoelectrochemical applications. *Nano Energy* 15, 353–361. doi: 10.1016/j.nanoen.2015.04.012

Cao, K., Jiang, Z., Zhang, X., Zhang, Y., Zhao, J., Xing, R. et al. (2015a). Highly water-selective hybrid membrane by incorporating g-$C_3N_4$ nanosheets into polymer matrix. *J. Membr. Sci.*, 490, 72–83. doi: 10.1016/j.memsci.2015.04.050

Cao, S., Low, J., Yu, J., and Jaroniec, M. (2015b). Polymeric photocatalysts based on graphitic carbon nitride. *Adv. Mater.* 27, 2150–2176. doi: 10.1002/adma.201500033

Cazelles, R., Liu, J., and Antonietti, M. (2015). Hybrid $C_3N_4$/Fluorine-Doped Tin Oxide Electrode Transfers Hydride for 1, 4-NADH Cofactor regeneration. *ChemElectroChem* 2, 333–337. doi: 10.1002/celc.201402421

Chen, P., Wang, H., Liu, H., Ni, Z., Li, J., Zhou, Y. et al. (2019). Directional electron delivery and enhanced reactants activation enable efficient photocatalytic air purification on amorphous carbon nitride co-functionalized with O/La. *Appl. Catal. B* 242, 19–30. doi: 10.1016/j.apcatb.2018.09.078

Chen, X., Jun, Y.-S., Takanabe, K., Maeda, K., Domen, K., Fu, X. et al. (2009). Ordered mesoporous SBA-15 type graphitic carbon nitride: a semiconductor host structure for photocatalytic hydrogen evolution with visible light. *Chem. Mater.* 21, 4093–4095. doi: 10.1021/cm902130z

Chen, Z., Vorobyeva, E., Mitchell, S., Fako, E., Ortuño, M. A., López, N. et al. (2018a). A heterogeneous single-atom palladium catalyst surpassing homogeneous systems for Suzuki coupling. *Nat. Nanotechnol.* 13, 702–707. doi: 10.1038/s41565-018-0167-2

Chen, Z., Wang, H., Xu, J., and Liu, J. (2018b). Surface engineering of carbon nitride electrode by molecular cobalt species and their photoelectrochemical application. *Chem. Asian J.* 13, 1539–1543. doi: 10.1002/asia.201800487

Choi, C. H., Lin, L., Gim, S., Lee, S., Kim, H., Wang, X. et al. (2018). Polymeric carbon nitride with localized aluminum coordination sites as a durable and efficient photocatalyst for visible light utilization. *ACS Catal.* 8, 4241–4256. doi: 10.1021/acscatal.7b03512

Han, Q., Wang, B., Zhao, Y., Hu, C., and Qu, L. (2015). A graphitic-$C_3N_4$ "Seaweed" architecture for enhanced hydrogen evolution. *Angew. Chem. Int. Ed.* 54, 11433–11437. doi: 10.1002/anie.201504985

He, P., Tang, X., Chen, L., Xie, P., He, L., Zhou, H. et al. (2018). Patterned carbon nitride-based hybrid aerogel membranes via 3d printing for broadband solar wastewater remediation. *Adv. Funct. Mater.* 28:1801121. doi: 10.1002/adfm.201801121

Huang, J., Antonietti, M., and Liu, J. (2014). Bio-inspired carbon nitride mesoporous spheres for artificial photosynthesis: photocatalytic cofactor regeneration for sustainable enzymatic synthesis. *J. Mater. Chem. A* 2, 7686–7693. doi: 10.1039/C4TA00793J

Huang, P., Liu, W., He, Z., Xiao, C., Yao, T., Zou, Y. et al. (2018). Single atom accelerates ammonia photosynthesis. *Sci. China Chem.* 61, 1187–1196. doi: 10.1007/s11426-018-9273-1

Jiang, L. L., Wang, Z. K., Li, M., Zhang, C. C., Ye, Q. Q., Hu, K. H. et al. (2018). Passivated Perovskite Crystallization via g-$C_3N_4$ for high-performance solar cells. *Adv. Funct. Mater.* 28:1705875. doi: 10.1002/adfm.201705875

Jun, Y. S., Lee, E. Z., Wang, X., Hong, W. H., Stucky, G. D., and Thomas, A. (2013). From melamine-cyanuric acid supramolecular aggregates to carbon nitride hollow spheres. *Adv. Funct. Mater.* 23, 3661–3667. doi: 10.1002/adfm.201203732

Li, H., Huang, H., Wang, Z., Zheng, Z., Wang, P., Liu, Y. et al. (in press). *In situ* extract nucleate sites for the growth of free-standing carbon nitride films on various substrates. *Catal. Today*, doi: 10.1016/j.cattod.2019.02.022

Liao, Y., Zhu, S., Ma, J., Sun, Z., Yin, C., Zhu, C. et al. (2014). Tailoring the Morphology of g-$C_3N_4$ by self-assembly towards high photocatalytic performance. *ChemCatChem* 6, 3419–3425. doi: 10.1002/cctc.201402654

Lin, B., Yang, G., and Wang, L. (2019). Stacking-layer-number dependence of water adsorption in 3D ordered close-packed g-$C_3N_4$ nanosphere arrays for photocatalytic hydrogen evolution. *Angew. Chem. Int. Ed.* 131, 4635–4639. doi: 10.1002/ange.201814360

Liu, J., An, T., Chen, Z., Wang, Z., Zhou, H., Fan, T. et al. (2017a). Carbon nitride nanosheets as visible light photocatalytic initiators and crosslinkers for hydrogels with thermoresponsive turbidity. *J. Mater. Chem. A* 5, 8933–8938. doi: 10.1039/C7TA02923C

Liu, J., and Antonietti, M. (2013). Bio-inspired NADH regeneration by carbon nitride photocatalysis using diatom templates. *Energy Environ. Sci.* 6, 1486–1493. doi: 10.1039/C3EE40696B

Liu, J., Cazelles, R., Zhou, H., Galarneau, A., and Antonietti, M. (2014a). The bioinspired construction of an ordered carbon nitride array for photocatalytic mediated enzymatic reduction. *Phys. Chem. Chem. Phys.* 16, 14699–14705. doi: 10.1039/C4CP01348D

Liu, J., He, K., Wu, W., Song, T. B., and Kanatzidis, M. G. (2017b). *In situ* synthesis of highly dispersed and ultrafine metal nanoparticles from chalcogels. *J. Am. Chem. Soc.* 139:2900. doi: 10.1021/jacs.6b13279

Liu, J., Huang, J., Dontosova, D., and Antonietti, M. (2013a). Facile synthesis of carbon nitride micro-/nanoclusters with photocatalytic activity for hydrogen evolution. *RSC Adv.* 3, 22988–22993. doi: 10.1039/C3RA44490B

Liu, J., Huang, J., Zhou, H., and Antonietti, M. (2014b). Uniform graphitic carbon nitride nanorod for efficient photocatalytic hydrogen evolution and sustained photoenzymatic catalysis. *ACS Appl. Mater. Interfaces* 6, 8434–8440. doi: 10.1021/am501319v

Liu, J., Kelley, M. S., Wu, W., Banerjee, A., Douvalis, A. P., Wu, J. et al. (2016a). Nitrogenase-mimic iron-containing chalcogels for photochemical reduction of dinitrogen to ammonia. *Proc. Natl. Acad. Sci. U S A* 113:5530. doi: 10.1073/pnas.1605512113

Liu, J., Li, M., Wang, J., Song, Y., Jiang, L., Murakami, T. et al. (2009). Hierarchically macro-/mesoporous Ti-Si oxides photonic crystal with highly efficient photocatalytic capability. *Environ. Sci. Technol.* 43, 9425–9431. doi: 10.1021/es902462c

Liu, J., Liu, G., Li, M., Shen, W., Liu, Z., Wang, J. et al. (2010). Enhancement of photochemical hydrogen evolution over Pt-loaded hierarchical titania photonic crystal. *Energy Environ. Sci.* 3, 1503–1506. doi: 10.1039/C0EE00116C

Liu, J., Liu, Y., Liu, N., Han, Y., Zhang, X., Huang, H. et al. (2015a). Metal-free efficient photocatalyst for stable visible water splitting via a two-electron pathway. *Science* 347, 970–974. doi: 10.1126/science.aaa3145

Liu, J., Wang, H., and Antonietti, M. (2016b). Graphitic carbon nitride "reloaded": emerging applications beyond (photo)catalysis. *Chem. Soc. Rev.* 45, 2308–2326. doi: 10.1039/c5cs00767d

Liu, J., Wang, H., Chen Zu, P., Moehwald, H., Fiechter, S., Van De Krol, R. et al. (2015b). Microcontact-printing-assisted access of graphitic carbon nitride films with favorable textures toward photoelectrochemical application. *Adv. Mater.* 27, 712–718. doi: 10.1002/adma.201404543

Liu, J., Yang, Q., Yang, W. T., Li, M. Z., and Song, Y. L. (2013b). Aquatic plant inspired hierarchical artificial leaves for highly efficient photocatalysis. *J. Mater. Chem. A* 1, 7760–7766. doi: 10.1039/C3TA11355H

Liu, Y., Wang, J., and Yang, P. (2016c). Photochemical reactions of g-$C_3N_4$-based heterostructured composites in Rhodamine B degradation under visible light. *RSC Adv.* 6, 34334–34341. doi: 10.1039/C6RA04430A

Liu, Z., Wang, G., Chen, H.-S., and Yang, P. (2018). An amorphous/crystalline g-$C_3N_4$ homojunction for visible light photocatalysis reactions with superior activity. *Chem. Commun.* 54, 4720–4723. doi: 10.1039/C8CC01824C

Lu, X., Liu, Z., Li, J., Zhang, J., and Guo, Z. (2017). Novel framework g-$C_3N_4$ film as efficient photoanode for photoelectrochemical water splitting. *Appl. Catal. B* 209, 657–662. doi: 10.1016/j.apcatb.2017.03.030

Lv, X., Cao, M., Shi, W., Wang, M., and Shen, Y. (2017). A new strategy of preparing uniform graphitic carbon nitride films for photoelectrochemical application. *Carbon* 117, 343–350. doi: 10.1016/j.carbon.2017.02.096

Martha, S., Nashim, A., and Parida, K. (2013). Facile synthesis of highly active g-$C_3N_4$ for efficient hydrogen production under visible light. *J. Mater. Chem. A* 1, 7816–7824. doi: 10.1039/C3TA10851A

Ong, W.-J. (2017). 2D/2D graphitic carbon nitride (g-$C_3N_4$) heterojunction nanocomposites for photocatalysis: why does face-to-face interface matter? *Front. Mater.* 4:11. doi: 10.3389/fmats.2017.00011

Ong, W. J., Tan, L. L., Ng, Y. H., Yong, S. T., and Chai, S. P. (2016). Graphitic carbon nitride (g-$C_3N_4$)-based photocatalysts for artificial photosynthesis and environmental remediation: are we a step closer to achieving sustainability? *Chem. Rev.* 116, 7159–7329. doi: 10.1021/acs.chemrev.6b00075

Peng, G., Xing, L., Barrio, J., Volokh, M., and Shalom, M. (2018). A General synthesis of porous carbon nitride films with tunable surface area and photophysical properties. *Angew. Chem. Int. Ed.* 130:1186. doi: 10.1002/anie.201711669

Ruan, Q., Luo, W., Xie, J., Wang, Y., Liu, X., Bai, Z. et al. (2017). A nanojunction polymer photoelectrode for efficient charge transport and separation. *Angew. Chem. Int. Ed.* 56, 8221–8225. doi: 10.1002/anie.201703372

Shalom, M., Gimenez, S., Schipper, F., Herraiz-Cardona, I., Bisquert, J., and Antonietti, M. (2014). Controlled carbon nitride growth on surfaces for hydrogen evolution electrodes. *Angew. Chem. Int. Ed.* 53, 3654–3658. doi: 10.1002/anie.201309415

Shan, X., Sui, N., Liu, W., Liu, M., and Liu, J. (2019). *In-situ* generation of supported palladium nanoparticles from a pd/sn/s chalcogel and applications in 4-nitrophenol reduction and suzuki coupling. *J. Mater. Chem. A.* 7, 4446–4450. doi: 10.1039/C8TA11772A

Sheng, X., Liu, Z., Zeng, R., Chen, L., Feng, X., and Jiang, L. (2017). Enhanced photocatalytic reaction at air-liquid-solid joint interfaces. *J. Am. Chem. Soc.* 139:12402. doi: 10.1021/jacs.7b07187

Sun, J., Zhang, J., Zhang, M., Antonietti, M., Fu, X., and Wang, X. (2012). Bioinspired hollow semiconductor nanospheres as photosynthetic nanoparticles. *Nat. Commun.* 3:1139. doi: 10.1038/ncomms2152

Thomas, A., Fischer, A., Goettmann, F., Antonietti, M., Müller, J.-O., Schlögl, R. et al. (2008). Graphitic carbon nitride materials: variation of structure and morphology and their use as metal-free catalysts. *J. Mater. Chem.* 18, 4893–4908. doi: 10.1039/B800274F

Wang, X., Maeda, K., Thomas, A., Takanabe, K., Xin, G., Carlsson, J. M. et al. (2009). A metal-free polymeric photocatalyst for hydrogen production from water under visible light. *Nat. Mater.* 8, 76–80. doi: 10.1038/NMAT2317

Wang, Y., Wang, X., and Antonietti, M. (2012). Polymeric graphitic carbon nitride as a heterogeneous organocatalyst: from photochemistry to multipurpose catalysis to sustainable chemistry. *Angew. Chem. Int. Ed.* 51, 68–89. doi: 10.1002/anie.201101182

Wenzel, R. N. (1936). Resistance of solid surfaces to wetting by water. *Ind. Eng. Chem.* 28, 988–994. doi: 10.1021/ie50320a024

Wu, Y., Feng, J., Gao, H., Feng, X., and Jiang, L. (2018). Superwettability-based interfacial chemical reactions. *Adv. Mater.* 31:1800718 doi: 10.1002/adma.201800718

Xia, P., Zhu, B., Cheng, B., Yu, J., and Xu, J. (2017). 2D/2D g-$C_3N_4$/$MnO_2$ nanocomposite as a direct Z-scheme photocatalyst for enhanced photocatalytic activity. *ACS Sustainable Chem. Eng.* 6, 965–973. doi: 10.1021/acssuschemeng.7b03289

Xiao, K., Chen, L., Chen, R., Heil, T., Lemus, S. D. C., Fan, F. et al. (2019). Artificial light-driven ion pump for photoelectric energy conversion. *Nat. Commun.* 10:74. doi: 10.1038/s41467-018-08029-5

Xiao, K., Giusto, P., Wen, L., Jiang, L., and Antonietti, M. (2018). Nanofluidic ions transport and energy conversion through ultrathin free-standing polymeric carbon nitride membranes. *Angew. Chem. Int. Ed.* 57, 10123–10126. doi: 10.1002/anie.201804299

Xiong, T., Cen, W., Zhang, Y., and Dong, F. (2016). Bridging the g-$C_3N_4$ interlayers for enhanced photocatalysis. *ACS Catal.* 6, 2462–2472. doi: 10.1021/acscatal.5b02922

Xiong, W., Chen, S., Huang, M., Wang, Z., Lu, Z., and Zhang, R. (2018). Crystal-face tailored graphitic carbon nitride films for high-performance photoelectrochemical cells. *Chemsuschem* 11, 2497–2501. doi: 10.1002/cssc.201801295

Xu, J., Cao, S., Brenner, T., Yang, X., and Shalom, M. (2015a). Supramolecular chemistry in molten sulfur: preorganization effects leading to marked enhancement of carbon nitride photoelectrochemistry. *Adv. Funct. Mater.* 25, 6265–6271. doi: 10.1002/adfm.201502843

Xu, J., Herraiz-Cardona, I., Yang, X., Gimenez, S., Antonietti, M., and Shalom, M. (2015b). The complex role of carbon nitride as a

sensitizer in photoelectrochemical cells. *Adv. Opt. Mater.* 3, 1052–1058. doi: 10.1002/adom.201500010

Xu, J., and Shalom, M. (2019). Conjugated carbon nitride as an emerging luminescent material: quantum dots, thin films and their applications in imaging, sensing, optoelectronic devices and photoelectrochemistry. *ChemPhotoChem.* doi: 10.1002/cptc.201800256

Xu, J., Shalom, M., Piersimoni, F., Antonietti, M., Neher, D., and Brenner, T. J. (2015c). Color-tunable photoluminescence and nir electroluminescence in carbon nitride thin films and light-emitting diodes. *Adv. Opt. Mater.* 3, 913–917. doi: 10.1002/adom.201500019

Xu, J., Thomas, J. K., B., Chabanne, L., Neher, D., Antonietti, M. et al. (2014). Liquid-based growth of polymeric carbon nitride layers and their use in a mesostructured polymer solar cell with V(oc) exceeding 1 V. *J. Am. Chem. Soc.* 136, 13486–13489. doi: 10.1021/ja508329c

Xu, J., Zhou, H., Shi, K., Yan, R., Tang, Y., Liu, J. et al. (2017). Bio-directed morphology engineering towards hierarchical 1D to 3D macro/meso/nanoscopic morph-tunable carbon nitride assemblies for enhanced artificial photosynthesis. *J. Mater. Chem. A* 5, 2195–2203. doi: 10.1039/c6ta08691h

Yang, Q., Li, M., Liu, J., Shen, W., Ye, C., Shi, X. et al. (2012). Hierarchical $TiO_2$ photonic crystal spheres prepared by spray drying for highly efficient photocatalysis. *J. Mater. Chem. A* 1, 541–547. doi: 10.1039/C2TA00060A

Yang, Q., Liu, J., Li, H., Li, Y., Hou, J., Li, M. et al. (2015a). Bio-inspired double-layer structure artificial microreactor with highly efficient light harvesting for photocatalysts. *RSC Adv.* 5, 11096–11100. doi: 10.1039/C4RA15943H

Yang, X., Tang, H., Xu, J., Antonietti, M., and Shalom, M. (2015b). Silver phosphate/graphitic carbon nitride as an efficient photocatalytic tandem system for oxygen evolution. *ChemSusChem* 8, 1350–1358. doi: 10.1002/cssc.201403168

Ye, L., and Chen, S. (2016). Fabrication and high visible-light-driven photocurrent response of g-$C_3N_4$ film: the role of thiourea. *Appl. Surf. Sci.* 389, 1076–1083. doi: 10.1016/j.apsusc.2016.08.038

Yu, H., Shi, R., Zhao, Y., Bian, T., Zhao, Y., Zhou, C. et al. (2017). Alkali-Assisted synthesis of nitrogen deficient graphitic carbon nitride with tunable band structures for efficient visible-light-driven hydrogen evolution. *Adv. Mater.* 29:1605148. doi: 10.1002/adma.201605148

Zhang, G., Li, G., Heil, T., Zafeiratos, S., Savateev, A., Wang, X. et al. (2019). Tailoring grain boundary chemistry of polymeric carbon nitride for enhanced solar $h_2$ production and $co_2$ reduction. *Angew. Chem. Int. Ed.* 11, 3471–3475. doi: 10.1002/ange.201811938

Zhang, J., Zhang, M., Lin, L., and Wang, X. (2015). Sol processing of conjugated carbon nitride powders for thin-film fabrication. *Angew. Chem. Int. Ed.* 54, 6297–6301. doi: 10.1002/anie.201501001

Zhang, X., Xie, X., Wang, H., Zhang, J., Pan, B., and Xie, Y. (2012). Enhanced photoresponsive ultrathin graphitic-phase $C_3N_4$ nanosheets for bioimaging. *J. Am. Chem. Soc.* 135, 18–21. doi: 10.1021/ja308249k

Zhang, Y., Mori, T., Ye, J., and Antonietti, M. (2010). Phosphorus-doped carbon nitride solid: enhanced electrical conductivity and photocurrent generation. *J. Am. Chem. Soc.* 132, 6294–6295. doi: 10.1021/ja101749y

Zhao, G., Yang, H., Liu, M., and Xu, X. (2018). Metal-free graphitic carbon nitride photocatalyst goes into two-dimensional time. *Front. Chem.* 6:551. doi: 10.3389/fchem.2018.00551

Zhao, Y., Liu, Z., Chu, W., Song, L., Zhang, Z., Yu, D. et al. (2008). Large-scale synthesis of nitrogen-rich carbon nitride microfibers by using graphitic carbon nitride as precursor. *Adv. Mater.* 20, 1777–1781. doi: 10.1002/adma.200702230

Zhou, H., Li, P., Liu, J., Chen, Z., Liu, L., Dontsova, D. et al. (2016). Biomimetic polymeric semiconductor based hybrid nanosystems for artificial photosynthesis towards solar fuels generation via $CO_2$ reduction. *Nano Energy* 25, 128–135. doi: 10.1016/j.nanoen.2016.04.049

**Conflict of Interest Statement:** The authors declare that the research was conducted in the absence of any commercial or financial relationships that could be construed as a potential conflict of interest.